Nanoscale Advances

ROYAL SOCIETY OF CHEMISTRY

PAPER

View Article Online
View Journal | View Issue

Cite this: *Nanoscale Adv.*, 2024, **6**, 2104

Assessment of laser-synthesized Si nanoparticle effects on myoblast motility, proliferation and differentiation: towards potential tissue engineering applications†

Clarissa Murru,[a] Lucas Duvert,[ab] Frederique Magdinier,[b] Adrien Casanova,[a] Anne-Patricia Alloncle,[a] Stefano Testa *[b] and Ahmed Al-Kattan *[a]

Due to their biocompatibility and biodegradability and their unique structural and physicochemical properties, laser-synthesized silicon nanoparticles (Si-NPs) are one of the nanomaterials which have been most studied as potential theragnostic tools for non-invasive therapeutic modalities. However, their ability to modulate cell behavior and to promote proliferation and differentiation is still very little investigated or unknown. In this work, ultrapure ligand free Si-NPs of 50 ± 11.5 nm were prepared by femtosecond (fs) laser ablation in liquid. After showing the ability of Si-NPs to be internalized by murine C2C12 myoblasts, the cytotoxicity of the Si-NPs on these cells was evaluated at concentrations ranging from 14 to 224 μg mL^{-1}. Based on these findings, three concentrations of 14, 28 and 56 μg mL^{-1} were thus considered to study the effect on myoblast differentiation, proliferation and motility at the molecular and phenotypical levels. It was demonstrated that up to 28 μg mL^{-1}, the Si-NPs are able to promote the proliferation of myoblasts and their subsequent differentiation. Scratch tests were also performed revealing the positive Si-NP effect on cellular motility at 14 and 28 μg mL^{-1}. Finally, gene expression analysis confirmed the ability of Si-NPs to promote proliferation, differentiation and motility of myoblasts even at very low concentration. This work opens up novel exciting prospects for Si-NPs made by the laser process as innovative tools for skeletal muscle tissue engineering in view of developing novel therapeutic protocols for regenerative medicine.

Received 20th November 2023
Accepted 23rd February 2024

DOI: 10.1039/d3na01020a

rsc.li/nanoscale-advances

1 Introduction

The possibility of monitoring cell behaviour and fate can dramatically help in the development of novel tissue engineering technology and therapeutic protocols in view of repairing and regenerating damaged tissues, occurring after injury or other degenerative diseases.[1] In this context, several approaches are currently investigated, including bio-inspired surface topography,[2] engineered functional nanoparticles[3,4] and chemical surface functionalization.[5] Similarly, due to their particular physicochemical properties (size, porosity, hydrophobicity, chemical composition, *etc.*), nanoparticles (NPs) have attracted great interest in the design of innovative theragnostic tools for drug delivery,[6] cell tracking[7,8] and therapy[9,10] with a particular focus on non-invasive anticancer therapeutics (*e.g.*, light-induced generation of singlet oxygen and related photodynamic therapy, radio frequency-induced hyperthermia, *etc.*).[11] On the other hand, their ultra-small size, down to 100 nm, and their high surface reactivity could offer remarkable interactions with biological environments which can be evaluated for their ability to modulate cell behaviour or to influence aspects such as cell differentiation and proliferation.[12,13] The control of the different cellular mechanisms listed above can both improve the fabrication of innovative nanocomposite materials for biomedical applications and promote the use of improved strategies towards therapeutic protocols in order to restore functionality of tissues damaged due to trauma, degenerative diseases or aging.[14] To date, several types of NPs based on polymers, metals and ceramics have been investigated in this respect; most of these studies were thus performed using a variety of stem cells including induced pluripotent stem cells (iPSCs).[15–18] For instance, Au-NPs functionalized with citrate, chitosan or fibronectin, are able to enhance the differentiation of human mesenchymal stem cells (MSCs) and adipose-derived stem cells (ADSCs), respectively, into cardiomyocytes and osteoblasts.[19,20] Ag-NPs can promote osteogenic differentiation of human urine-derived stem cells (USCs) and the proliferation of MSCs,[21] while graphene-based NPs enhance the

[a]*Aix-Marseille University, CNRS, LP3 UMR 7341, Campus de Luminy, C13288, Marseille, France. E-mail: ahmed.al-kattan@univ-amu.fr*

[b]*Aix-Marseille University, INSERM, MMG, Marseille Medical Genetics, 13385 Marseille, France. E-mail: stefano.testa@univ-amu.fr*

† Electronic supplementary information (ESI) available. See DOI: https://doi.org/10.1039/d3na01020a

cardiomyogenic and angiogenic differentiation capacity of MSCs for cardiac tissue regeneration.[22] Due to their biocompatibility and biodegradability, SiO_2-NPs were also investigated for their ability to modulate murine myoblast (C2C12) behaviour by improving the differentiation of C2C12 myoblasts into myotubes with a beneficial effect on muscle growth.[23] Despite these promising results, the major concerns about the NPs employed in these research studies are their conventional chemical and electrochemical production methods, which involve hazardous products (*e.g.*, HF, nitrate salts, chloride, citrate, *etc.*) and various ligands. The presence of potentially dangerous reagents generally leads to surface contamination by residual toxic products, which can negatively influence the interaction with the biological matrix.[24] Moreover, in some cases the elaboration of NPs takes place under extreme physicochemical conditions (*e.g.*, pH, pressure, temperature, *etc.*) which requires a rigorous control of the synthesis procedure. These reactions frequently necessitate different organic solvents (*e.g.*, ethanol, THF, *etc.*) leading to switching steps between organic and aqueous solutions that complicates the fabrication and purification procedures.[25] Driven by its flexibility, simplicity and rapidity, we have recently introduced an ultra-short femtosecond (fs) laser ablation approach in liquid as a relevant process to design ultra-pure crystalline NPs for biomedical applications. Thanks to the interaction of a fs laser beam with a solid target initially immersed in a liquid, this method allows the formation of nanoclusters which coalesce in a liquid medium to produce a very stable colloidal NP solution.[26] Moreover, by playing with several parameters of the laser (*e.g.*, fluence, beam time duration, ablation/fragmentation sequence, *etc*), the possibility to monitor their physicochemical properties including size, size-distribution and chemical composition has been demonstrated.[27,28] In this context, we have recently used Si (silicon), already known to be involved in many physiological activities such as bone mineralization[29] and transduction mechanisms,[30] to elaborate Si-NPs by fs laser ablation in liquid for biomedical applications. Our study proved their biocompatibility and biodegradability into orthosilicic acid $Si(OH)_4$ without specific induced toxicity.[31] We thus demonstrated their complete safety properties thanks to systematic *in vitro* and *in vivo* tests,[32] while their therapeutic potential was assessed by a variety of non-invasive testes including intra-tumour radiofrequency (RF)-induced hyperthermia[33] and two-photon excited photodynamic therapy (TPE-PDT).[34] Furthermore, we tested Si-NPs as functional additives in innovative electrospun-nanofiber platforms for tissue engineering applications.[35] Nanoparticles can lead to the development of novel tissue engineering technologies and therapeutic protocols to regenerate damaged tissues. Hence, their ability to modulate different aspects of cellular programs is still very little investigated or unknown. In this work, we assessed the effect of laser-synthesized Si-NPs on murine C2C12 myoblast differentiation, proliferation and motility both at the molecular and phenotypical levels. This work is conceived as a first step towards the possible use of these types of Si-NPs in skeletal muscle cells for future applications in tissue engineering and regenerative medicine.

2 Materials and methods

2.1 Synthesis of Si-NPs and characterization

Fabrication of the Si-NPs was carried out with a femtosecond laser (Light Conversion Carbide CB1-05 Yb:KGW), working with a pulse duration of 430 fs, an energy per pulse of 40.3 μJ and a repetition rate of 10 kHz at 1028 nm. Precisely, a Si wafer was placed at the bottom of a glass vessel filled with 10 mL of ultrapure water, and then subjected to a fs laser beam for 10 min with a fluence of 5.081 J cm^{-2}. To promote optimal surface ablation, a scanner system was coupled with the fs laser beam. The characterization of the structural properties of the Si-NPs was achieved through a high-resolution transmission electron microscopy (HR-TEM) system (JEOL JEM 3010) in imaging and diffraction modes working at 200 kV. In parallel dynamic light scattering (DLS) measurements were also performed on Si-NPs solution with a Zetasizer Nano ZS instrument (Malvern Instruments) to assess their hydrodynamic size and zeta potential surface charge. To proceed to biological *in vitro* studies, calibrated Si-NP solutions at increased concentrations in the range of 14 to 224 μg mL^{-1} were prepared through a centrifugation process (14 200 rpm for 10 min). The concentration of the Si-NPs was measured by an inductively coupled plasma mass spectrometry (ICP-MS) method.

2.2 Cell cultures

Murine myoblasts C2C12 (ATCC) were cultured according to a previously published protocol[36] in T-75 Flasks (Sarstedt) at 37 °C and 5% CO_2 in DMEM GlutaMAX (Gibco) supplemented with 10% heat-inactivated fetal bovine serum (FBS, EuroClone), penicillin (100 IU mL^{-1}, Gibco), and streptomycin (100 mg mL^{-1}, Gibco). To stimulate differentiation, once 90% confluency was reached, cells were transferred to differentiation medium (DM) composed of DMEM GlutaMAX (Gibco) supplemented with 2% horse serum (Gibco). The images and counting of the cells were obtained with a reverse microscope (EVOS M5000, Invitrogen, Thermo Fisher, America).

2.3 Cell survival assay

For cell survival assays, C2C12 cells were seeded in 12-well plates (Thermo Scientific) at 5×10^4 cells per well respectively. After 24 h, the culture medium was replaced by 1 mL of fresh medium containing different concentrations of Si-NPs (14 to 224 μg mL^{-1}). After 72 h of exposure, cell viability was determined by MTT (3-(4,5-dimethylthiazol-2-yl)-2,5-diphenyltetrazolium bromide) colorimetric assay. This test is based on the reduction of the tetrazolium salt by the mitochondria of living cells. The absorbance measured at 600 nm is proportional to the number of living cells.

2.4 Differentiation assay

The fusion index (FI) is defined as the ratio between the number of nuclei included in myosin heavy chain-expressing cells (containing at least three nuclei) and the number of nuclei for each field. To assess the influence of Si-NPs on C2C12 myoblast

myogenic differentiation,[37] FI was manually calculated using Fiji software, on samples prepared as described below. C2C12 cells were seeded into 12-well plates (Thermo Scientific) at 10^5 cells per well. After 24 h the culture medium was replaced by 1 mL of fresh medium containing different concentrations of Si-NPs (0, 14, 28, and 56 μg mL^{-1}). After 48 h the cells reached adequate confluence (90%), and the medium was replaced with a differentiation medium to induce myotube formation. DM was changed every 48 h for up to 1 week, to allow for proper myogenic differentiation. Then, after rinsing medium residues with PBS, cells were fixed with 4% paraformaldehyde in PBS at 4 °C for 10 min and stored at 4 °C for subsequent immunofluorescence analysis.

2.5 Immunofluorescence analysis

The samples were analyzed by immunofluorescence according to a previously described protocol.[38] Briefly, cells were permeabilized in a solution of Triton X-100 0.3% in PBS for 1 h at room temperature (RT) and blocked with a blocking solution consisting of 10% goat serum, 1% glycine, and 0.1% Triton X-100 in PBS for 1 h at RT. Subsequently, the cells were incubated with mouse monoclonal anti-myosin heavy chain (MF20, DHSB) primary antibody, diluted 1 : 100 in a blocking solution for 2 h at RT and then rinsed with a washing solution consisting of 1% bovine serum albumin (BSA) and 0.2% Triton X-100 in PBS. After washing, the cells were incubated with Alexa Fluor 555-conjugated goat anti-mouse IgG secondary antibody (H + L; Thermo Fisher Scientific, diluted 1 : 400) for 1 h. Finally, the nuclei were counterstained with 300 nM DAPI (Thermo Fisher Scientific) in PBS for 10 min.

2.6 Sample preparation for high-resolution scanning electron microscopy imaging (HR-SEM) coupled with energy dispersive X-ray (EDX) analysis

The adhesion of the Si-NPs to the cell wall was monitored through images obtained using HR-SEM (Jeol JSM-7900F) working at 30 kV. C2C12 myoblasts were seeded on glass coverslips (10^5 per sample) and 24 h later exposed to 56 μg mL^{-1} Si-NPs for 72 h. Then, the culture medium was removed and the cells were washed 3 times with PBS in order to eliminate the NPs in the suspension. Subsequently, the samples were fixed with 5% glutaraldehyde solution over 2 h, then washed with increasing concentrations of ethanol (25, 50, 75, and 95%) and finally stored at 2 °C until analysis. HR-SEM coupled with EDX measurements were also performed on cell sections of C2C12 cells to confirm Si-NP internalization. Basically, C2C12 myoblasts were seeded in 6-well plates (Thermo Scientific) (10^5 per sample) and 24 h later exposed to 56 μg mL^{-1} Si-NPs for 72 h. The culture medium was removed and the cells were washed with a 0.1 M phosphate buffer solution. Subsequently the myoblasts were fixed with 2 mL of a glutaraldehyde 2.5% and 0.1 M phosphate buffer mixture for one hour under gentle stirring conditions. After the removal of glutaraldehyde, the samples were washed and fixed with 2 mL of a 1% osmium solution diluted in phosphate buffer and kept in total darkness for 30 minutes. Several washing steps were then carried out with increasing concentrations of ethanol (50, 70, 80, 90, and 100%) in order to promote a gradual dehydration of the specimens. The fixed and dehydrated cells were finally removed from the multi-well plate, soaked in the resin and polymerized at 60° for 24 hours. The use of a microtome cutter and a diamond blade was crucial to obtain resin segments with a thickness of 30 μm that allow the analysis of cell sections which were deposited on TEM grids to perform SEM analysis. EDX measurements were performed to confirm the chemical nature of the Si-NPs detected.

2.7 Proliferation assay

Growth curves were obtained according to Testa *et al.*[39] method. Briefly, C2C12 cells were seeded into 24-well plates (Thermo Scientific) at 10^4 cells per well. Three wells were prepared for each experimental time point (1, 3, 6, and 8 days) and each Si-NP concentration (0, 14, 28, and 56 μg mL^{-1}). Cellular proliferation was evaluated by harvesting cells at each time point and calculating the average cell number by means of a Burker counting chamber.

2.8 Scratch-wound healing assay

Scratch-wound assays were performed according to the Gargioli *et al.* study.[40] C2C12 cells were seeded in 12-well plates (Thermo Scientific) at 10^5 cells per well. Three wells for each concentration of Si-NPs (0, 14, 28, and 56 μg mL^{-1}) were prepared. After 48 h, the confluent C2C12 monolayer was scratched by using a 10 μL pipette tip. The cells were washed with DMEM (Gibco) to remove any detached cells, and 1 mL of fresh medium containing the right concentration of Si-NPs was added. Time lapse imaging was recorded for each well, taking photographs every 30 minutes for 24 hours.

2.9 Quantitative RT-PCR analysis

C2C12 cells were seeded in 6-well plates (Thermo Scientific) at 3 × 10^5 cells per well, with three wells for each concentration of Si-NPs (0, 14, 28, and 56 μg mL^{-1}) and each experimental time point (early – 80% of cell confluence – day 1; medium – 100% of cell confluence – day 2; late – differentiated myotubes – day 4). Once full confluence was reached (medium point), the growth medium was changed to the differentiation medium, to allow the correct differentiation of myoblasts. RNA was extracted using an RNeasy mini kit (Qiagen), and then 2 μg of RNA for each sample was retrotranscribed using SuperScript IV reverse transcriptase (Invitrogen), according to the manufacturers' instructions. Glyceraldehyde 3-phosphate dehydrogenase (GAPDH) was selected as the endogenous control after verifying its stable expression. Quantitative RT-PCR analysis was performed with a QuantStudio™ 5 Real-Time PCR System (96-wells, Applied Biosystems). Each cDNA sample was amplified using a LightCycler 480 SYBR Green I Master (Roche). Relative mRNA levels were calculated by the delta CT method (ΔΔCt).[41] Primer specificity was confirmed by melting curve analysis.

The primers used are listed below:

(1) GAPDH (80): Fw: ACTGAGCAAGAGAGGCCCTA; Rv: TATGGGGGTCTGGGATGGAA

(2) MHC (85): Fw: AACTGAAGAATGCCTATGAAG; Rv: TCTGCTATCTCTTGTTCTAAGT

(3) MyoD1 (82): Fw: GGAAGGGAAGAGCAGAAG; Rv: AAGGACTACAACAACAACAAC

(4) Desmin (82): Fw: CGTGACAACCTGATAGAC; Rv: TGTTCTCTGCTTCTTCTC

(5) Myomaker (94): Fw: GTTGCTTCACTCTGTTCA; Rv: TATTTACTGGTCTAGGGTTCT

(6) MKi67 (75): Fw: GGCATTCACAGCAACTTA; Rv: CACCTTCATCCAGATTCAC

(7) C-met (148): Fw: AGTCCTATATTGATGTCTTAC; Rv: AACCTGATTATTCTTGTATGA

2.10 Statistical analysis

All experiments were performed at least in biological triplicate. Data were analyzed using GraphPad Prism 8, and values were expressed as means ± standard error. Statistical significance was tested using one-way ANOVA tests with the appropriate multiple comparison tests. A probability of less than 5% ($p < 0.05$) was considered as statistically significant.

3 Results

3.1 Physicochemical characterization of Si-NPs

As described above, Si-NPs elaborated by the femtosecond laser process were characterised by HR-TEM coupled with X-ray diffraction measurements. As shown in Fig. 1, Si-NPs appeared typically spherical (Fig. 1a) with an average diameter of 50 ± 11.5 nm (Fig. 1b). Moreover, electron diffraction analysis confirmed the polycrystalline structure of Si-NPs with the presence of diffraction rings, corresponding to the (111), (220), and (311) and (331) crystalline planes of the cubic diamond structure (Fig. 1c).

ζ-Potential measurements were also carried out revealing negative surface −45 ± 1.5 mV due to partial oxidation of the surface. The concentration of Si-NPs was systematically determined by inductively coupled plasma mass spectroscopy (ICP-MS) at an average of 14 ± 1 μg mL^{-1}. To proceed to biological *in vitro* studies, calibrated Si-NP solutions at increased concentrations in the range of 14 to 224 μg mL^{-1} were prepared based on centrifugation at 14 200 rpm for 10 min. The value of 0 μg mL^{-1} of Si-NPs was taken as the control.

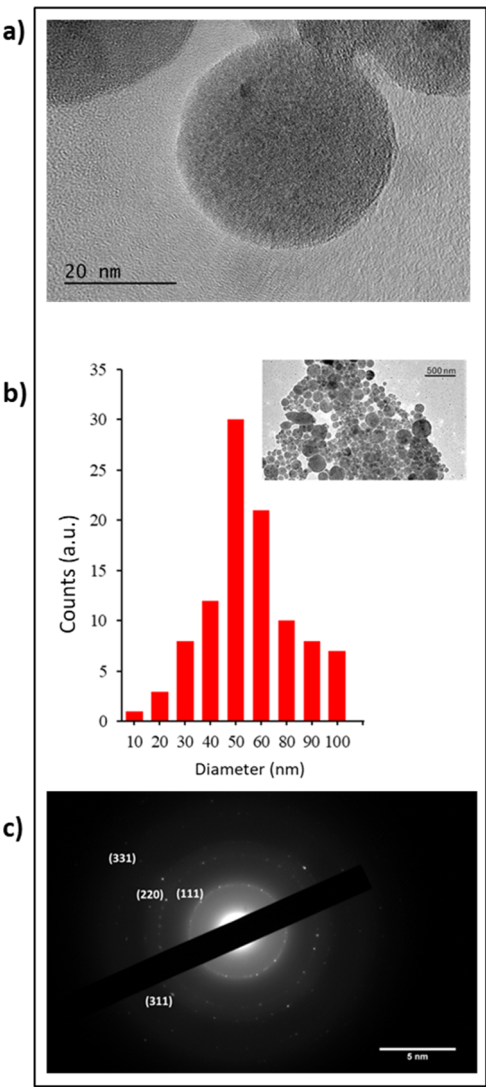

Fig. 1 Morphological characterization of Si-NPs. Si-NPs were characterized by HR-TEM analysis (a). Si-NP size distribution is displayed in histogram (b) where the bars show the percentage of Si-NPs for the different sizes indicated on the *x*-axis. (c) Electron diffraction pattern of Si-NPs.

3.2 *In vitro* cytotoxic assays

In order to evaluate the cytotoxic impact of Si-NPs on C2C12 myoblasts, cell survival was quantified by using the MTT colorimetric assay, which is used to evaluate the metabolic activity of mitochondria. C2C12 murine myoblasts were incubated for 72 h with different concentrations of Si-NPs ranging from 14 to 224 μg mL^{-1}. The cell viability profile shows a survival around 70% for a concentration of 28 μg mL^{-1} and 50% for a concentration of 56 μg mL^{-1}. However, higher concentrations of Si-NPs dramatically reduce cell survival to less than 20% at a concentration of 224 μg mL^{-1} (Fig. 2).

For this reason, further biological tests were performed in a range between 14 and 56 μg mL^{-1}. The mechanical adhesion and internalization of NPs into the myoblasts were investigated through SEM microscopy after fixation of the samples (Fig. 3). Before proceeding with the observation, the samples were

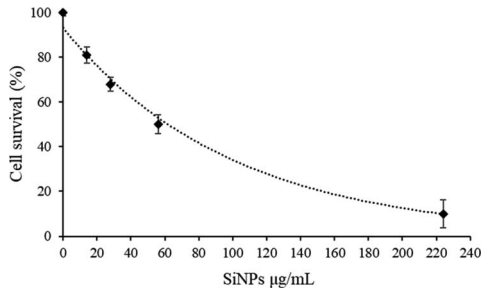

Fig. 2 MTT assay in C2C12 myoblasts. Cell viability was determined following exposure to different concentrations of Si-NPs (14–224 μg mL^{-1}, *x*-axis) for 72 h. The percentage of viable cells is indicated on the *y*-axis.

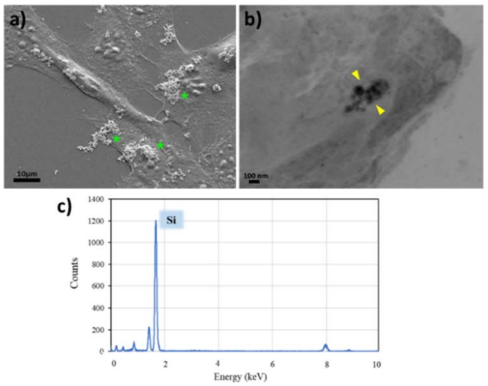

Fig. 3 Images of C2C12 internalization after 72 h of incubation with 56 μg mL^{-1} of Si-NPs. Si-NPs adhere to the cell surface (a) forming aggregates (see the green asterisk). Si-NPs internalized by the myoblasts (b, yellow arrow heads). EDX confirmed the presence of Si-NPs within the cells (c).

rinsed several times with ethanol and water to eliminate the excess non-adhered suspended nanoparticles. The absence of the solvent before fixation led to a rearrangement of the Si-NPs which tend to aggregate on the cell surface (Fig. 3a). By analysing cell sections, Si-NPs were also detected in the aggregate form, confirming the internalization of Si-NPs by the myoblast cells (Fig. 3b). In addition, EDX measurements were carried out in the sample fragment containing the NPs, confirming the presence of the silicon element related to the Si-NPs (Fig. 3c). The totality of the elements displayed on the spectrum derived from the composition of the resin and the reagents used for fixing the sample is provided in the ESI (ESI Fig. 1).†

3.3 Effects of the exposure to Si-NPs on C2C12 cellular processes

In order to evaluate the biological response of Si-NPs, C2C12 myoblasts were exposed to increasing doses of Si-NPs (14, 28, and 56 μg mL^{-1}). In particular, we evaluated the impact of Si-NPs on differentiation of myoblasts to myotubes, the proliferation of myoblasts and cellular motility. Myoblast differentiation is a highly controlled multistep process in which individual mononucleated myoblasts fuse to form multinucleated myotubes. Several genes are involved in this process and their transcription is finely regulated over time. Different types of nanoparticles can promote the formation of myotubes, as reported in the literature.[42,43] We first studied the influence of the exposure to different concentrations of Si-NPs on the differentiation of C2C12 cells by determining the fusion index (FI). The Si-NPs significantly increased the FI value for all concentrations tested compared to the control, with a higher FI obtained for a concentration of 28 μg mL^{-1} (Fig. 4a and b and ESI Table 1†).

The proliferation rate was calculated by analysing cell growth curves obtained during 8 days of continuous exposure to three concentrations of Si-NPs. The experiment was stopped on the eighth day when the cells reached confluence (Fig. 5).

Compared to controls, the treatment with the lowest concentration (14 μg mL^{-1}) did not change the proliferation rate. On the other hand, the highest concentration (56 μg mL^{-1}) significantly decreased the proliferation rate, in particular between day 3 and 6. At the medium range concentration (28 μg mL^{-1}), we observed a significant increase in cell number at day 3 compared to that of the control and to the two other concentrations tested (ESI Table 2† and Fig. 5). To assess whether the exposure to Si-NPs also affected the cellular motility, a scratch-wound healing assay was performed. The curves indicating the percentage of wound closure were obtained every 30 minutes for 24 hours by calculating the surface deprived of cells at each time point. We observed a trend with faster healing for the first two concentrations (14 and 28 μg mL^{-1}) with a closure of the wound between 6 and 21 hours post scratch, compared to the control (Fig. 6 and ESI Table 3†).

Consistent with the other observations on cell proliferation and cell differentiation, we observed a lower healing rate at a higher concentration (56 μg mL^{-1}) suggesting that a high concentration of Si-NPs might impair a number of cellular

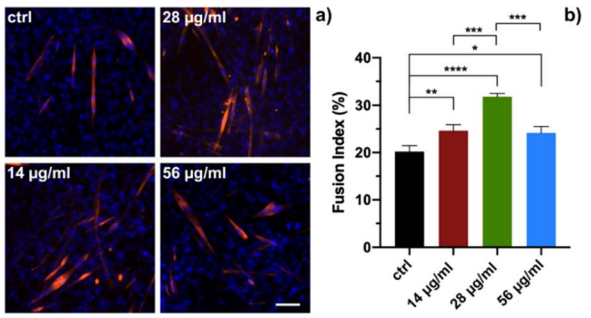

Fig. 4 Fusion index analysis. Representative immunofluorescence images under each experimental condition (a). Myotubes positive for the myosin heavy chain are stained in red, while nuclei are stained in blue with DAPI (scale bar = 50 μm). The graph displays the percentage of the fusion index of differentiated C2C12 myoblasts exposed to different concentrations of Si-NPs (b). Each bar represents an average of 3 independent experiments (for each experiment, $n = 6$ fields were analysed) with experimental variation displayed by error bars.

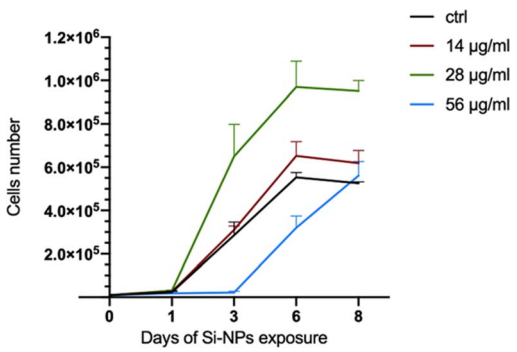

Fig. 5 Analysis of proliferation. Growth curves of C2C12 myoblasts exposed to increasing concentrations of Si-NPs for 8 days. The *x*-axis displays the number of days of Si-NP exposure. The *y*-axis displays the number of cells counted at each time point. Each time point is the average of 3 experiments with experimental variation displayed by error bars. A concentration of 28 μg mL^{-1} (green line) showed the highest proliferation rate.

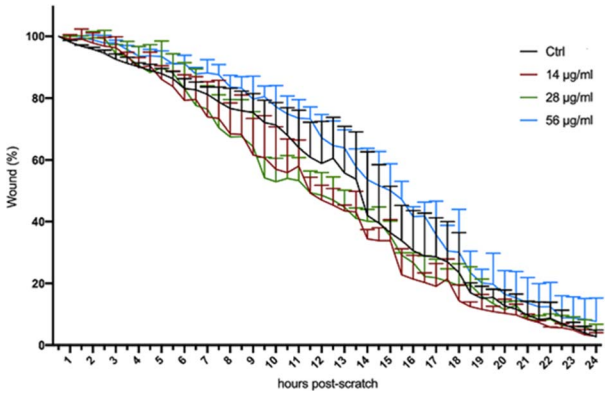

Fig. 6 Scratch-wound healing assay. The *y*-axis displays the percentage of wound at the surface of the culture plate. The *x*-axis displays the time of recording, 1 to 24 h post-scratch. The lines indicate the percentage of wound closure in 24 h for the different concentrations of Si-NPs tested. Each time point is the average of 3 experiments with experimental variation displayed by error bars.

processes together with cell viability. In order to evaluate the effect of the exposure to Si-NPs on the expression of genes related to muscle function, quantitative real-time PCR analysis (qRT-PCR) was performed on C2C12 cells. The expression levels of 6 genes (4 related to muscle differentiation, 1 to proliferation and 1 to cellular motility) were calculated for each concentration of Si-NPs tested (0, 14, 28 and 56 µg mL^{-1}), during three experimental time points (early, medium and late exposure). At the early stage (1 day post exposure to Si-NPs), no differences were observed between cells exposed to Si-NPs and controls for all genes studied. At the medium experimental point (3 days post exposure to Si-NPs), muscle-related genes started to be overexpressed under the 28 and 56 µg mL^{-1} conditions, with a significant increase in the expression of MyoD (the master gene of muscle differentiation) and desmin (28 µg mL^{-1}), an early marker of muscle differentiation. Myomaker (marker of the myotube fusion process) expression was higher for the samples exposed to 28 and 56 µg mL^{-1}, while expression of myosin heavy chain (MHC, a late marker of muscle differentiation) started to increase at a concentration of 28 µg mL^{-1} Si-NPs. Moreover, expression of Ki-67 (a marker of proliferation) and C-met (a marker of cellular motility) progressively increased for all concentrations tested, being significantly higher under the 28 and 56 µg mL^{-1} conditions. At the late stage (5 days post exposure), MyoD was significantly overexpressed under all conditions. Desmin and MHC expression also increased for all concentrations tested (being significantly higher only at 56 µg mL^{-1}) while Myomaker expression significantly increased at 14 and 56 µg mL^{-1}. The expression of the proliferation marker started to decrease at the first two concentrations, remaining significantly overexpressed at 56 µg mL^{-1}, while C-met expression strongly decreased for all the concentrations tested (Fig. 7 and ESI Table 4†).

The trend in the level of expression of each gene for each concentration of Si-NPs tested during the three experimental

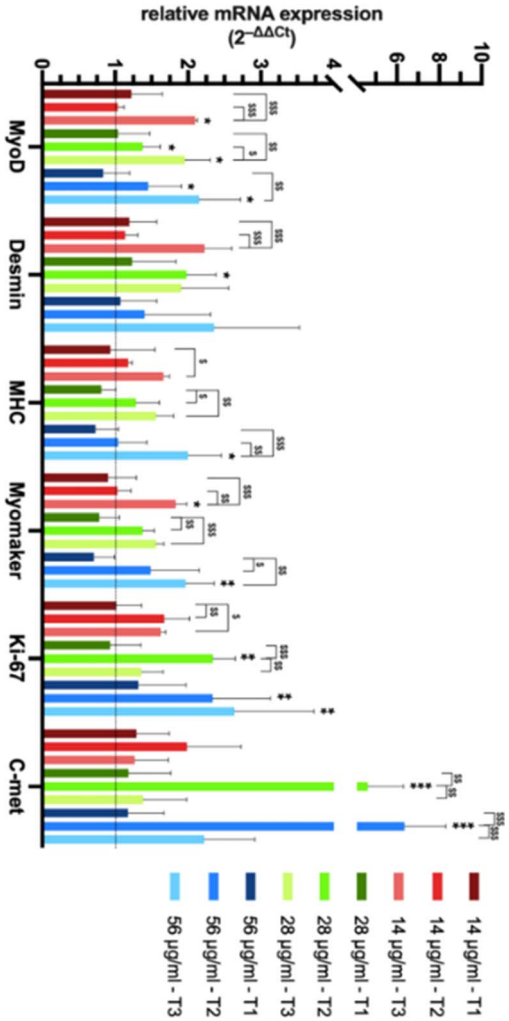

Fig. 7 Relative gene expression. The *y*-axis displays the relative values of the mRNA levels, calculated with the $2^{-\Delta\Delta Ct}$ method. Each bar is the average of 3 experiments with experimental variation displayed by error bars. The *x*-axis displays the genes studied for each concentration of Si-NPs at each experimental time point.

time points was also studied. Interestingly, the expression of muscle-related genes increased over time, while proliferation- and motility-related genes peaked in the medium stage, to decline in the late stage (Fig. 7). This significant trend in the kinetics of gene expression is consistent with a decrease in cell proliferation and migration associated with muscle commitment and differentiation (ESI Table 5†).

4 Discussion

In our previous studies we have shown the benefit of employing laser-synthesized Si-NPs as a potential biocompatible and biodegradable therapy tool for oncology applications.[31] In this context, it appears relevant to assess the effect of such NPs as novel functional additives on modulation of cell behavior and promotion of proliferation, differentiation and motility both at the molecular and phenotypical levels. The possibility of influencing cell behavior can be useful for developing therapeutic

protocols and models for tissue engineering applications. However, so far, the most widely used processes to obtain NPs involve the use of different solvents and multi-step approaches, resulting in time-consuming and expensive procedures that can lead to the chemical contamination of the NP surface, a condition that undermines their effect when applied to living matter. In this work, ultra-pure ligand free Si-NPs of 50 ± 11.5 nm were generated by a laser ablation process to by-pass such limitations. It has been largely studied and shown that the interaction between nanoparticles and cells triggers a cascade of molecular events which could induce toxicity and cell death.[44] These mechanisms are associated with the uptake of nanoparticles, their persistence at the cellular level, and their ability to release free radicals and to induce oxidative stress.[45] In our study cytotoxicity was maintained up to a limit of 56 μg mL^{-1} of Si-NPs with a cell survival of 50%, and their internalization was assessed by electron microscopy. At the extracellular membrane, NPs can interact with components of the plasma membrane or extracellular matrix to be internalized, mainly by endocytosis.[46] Shin-Woo Ha *et al.* demonstrated that once internalized, Si-NPs are quickly sequestered by the autophagosome, an organelle designed to isolate and eliminate potentially toxic agents. This internalization might generate a stress response that would in turn stimulate one or more of the common mitogen-activated protein kinase (MAPK) signaling pathway cascades that can lead to the conversion of extracellular stimuli into a wide range of cellular responses.[47] MAP kinase-associated signal transduction cascades are among the most thoroughly studied signal transduction systems and have been shown to participate in cell differentiation, cell movement, cell division, and cell death.[48,49] In this work we used a defined range of Si-NP concentrations to demonstrate their significant stimulatory effects on several cellular processes. The experiments conducted on cellular proliferation proved a positive influence of Si-NPs, with a proliferation rate after 8 days of continuous exposure which is almost the double compared to that of the controls (Fig. 5, 28 μg ml^{-1}). Gene expression analysis confirmed these data, showing a peak of Ki-67 expression at the medium experimental time point for each concentration of NPs tested, with a significant decrease at the late point (28 μg mL^{-1}) consistent with the full confluence of the cell monolayer and the switching to a differentiation medium, both known to promote exit from the replicative cycle (Fig. 7). The study of cellular motility was conducted by using a scratch-wound healing assay. This assay revealed a trend for the samples exposed to low and medium concentrations of Si-NPs to migrate to the wound area faster than the control (Fig. 6). Gene expression analysis confirmed this result, showing a common trend for each concentration used with a peak at the medium point and a strong decrease at the late point, when the surface of the wound is filled with cells. This effect is significantly higher at the medium and high concentrations (Fig. 7, C-met). Interestingly, while in the scratch-test assay, the best results are obtained with exposure to low and medium concentrations of Si-NPs, the most significant results were obtained for the medium and high concentrations regarding the quantification of gene expression. However, the sensitivity of the two approaches is different as the exposure time differs between the two experiments, 24 h for the scratch assay and 4 days for the qRT-PCR. Regarding myogenic differentiation, Si-NPs showed a robust positive effect at each concentration as indicated by the fusion index (Fig. 4) and confirmed by gene expression patterns. For qRT-PCR experiments, we summarized key steps of the myogenic program by observing the expression trend of 3 genes sequentially expressed during myoblast to myotube differentiation (MyoD, Desmin and MHC, repectively) and a marker of myoblast fusion (Myomaker). The results showed that each concentration of Si-NPs tested can increase the expression levels of each gene over time, with the more significantly relevant results obtained at 28 μg mL^{-1}. Of note, this concentration is the only one able to promote the overexpression of desmin at the medium point (Fig. 7). Overall, the results presented here confirm and deepen the observations regarding the positive effect of using Si-NPs to increase the myogenic capabilities of myoblasts, demonstrating a positive effect not only on differentiation but also on proliferation and migration. Interestingly, although each concentration of Si-NPs used for these experiments has proven to have a positive effect on the cellular fitness of C2C12 myoblasts, a concentration of 28 μg mL^{-1} yielded the best results when comparing the phenotypic and molecular experiments.

5 Conclusion

Here, the effect of ultra-pure ligand-free Si-NPs (50 ± 11.5 nm) obtained by fs laser ablation in liquid was evaluated. This research demonstrated the positive outcomes of the exposure of C2C12 myoblasts to Si-NPs, leading to significant improvements in their proliferation, differentiation and motility, even at the lowest concentration, both in phenotypic and molecular analyses. Si-NPs could be considered an optimal candidate as an alternative to classical growth and differentiation factors with interesting features: (i) excellent stability over time at room temperature; (ii) no species-specificity (abiotic factor); (iii) advantageous production procedures in terms of time and costs. Overall, the Si-NPs can be considered an useful and easy-to-use tool for biomedical investigation ranging from the establishment of novel differentiation protocols to tissue engineering applications.

Author contributions

C. M., S. T. and A. A. K. conceived the work; C. M., L. D. and A. A. K. designed and characterized the NPs; C. M., S. T. and F. M. performed biological experiments and analysed the obtained data. C. M., S. T., F. M. and A. A. K. wrote the manuscript. All authors reviewed the article, added comments and corrections in drafting the manuscript. All authors have read and agreed to the published version of the manuscript.

Conflicts of interest

The authors declare that they have no competing interest.

Acknowledgements

The work was funded by the French National Research Agency (ANR Medilibs and Diagem projects) together with the French Defence Innovation Agency (ANR—DGA/AID—ICELARE Project ID ANR—20—ASTR—0004). The authors express thanks to Damien Chaudenson and Alexandre Altié for their assistance in microscopy measurements and sample preparations.

References

1 F. Han, J. Wang, L. Ding, *et al.*, Tissue Engineering and Regenerative Medicine: Achievements, Future, and Sustainability in Asia, *Front. Bioeng. Biotechnol.*, 2020, **8**, 83, DOI: 10.3389/fbioe.2020.00083.

2 S. Arango-Santander, Bioinspired Topographic Surface Modification of Biomaterials, *Materials*, 2022, **15**(7), 2823, DOI: 10.3390/ma15072383.

3 G. R. Rudramurthy and M. K. Swamy, Potential applications of engineered nanoparticles in medicine and biology: an update, *JBIC, J. Biol. Inorg. Chem.*, 2018, **23**(8), 1185–1204, DOI: 10.1007/s00775-018-1600-6.

4 K. Upadhyay, R. K. Tamrakar, S. Thomas and M. Kumar, Surface functionalized nanoparticles: A boon to biomedical science, *Chem.-Biol. Interact.*, 2023, **380**, 110537, DOI: 10.1016/j.cbi.2023.110537.

5 A. Casanova, M. C. Blatche, C. A. Ferre, *et al.*, Self-Aligned Functionalization Approach to Order Neuronal Networks at the Single-Cell Level, *Langmuir*, 2018, **34**(22), 6612–6620, DOI: 10.1021/acs.langmuir.8b00529.

6 M. J. Mitchell, M. M. Billingsley, R. M. Haley, M. E. Wechsler, N. A. Peppas and R. Langer, Engineering precision nanoparticles for drug delivery, *Nat. Rev. Drug Discovery*, 2021, **20**(2), 101–124, DOI: 10.1038/s41573-020-0090-8.

7 J. Kim, P. Chhour, J. Hsu, *et al.*, Use of Nanoparticle Contrast Agents for Cell Tracking with Computed Tomography, *Bioconjugate Chem.*, 2017, **28**(6), 1581–1597, DOI: 10.1021/acs.bioconjchem.7b00194.

8 Q. Wang, X. Ma, H. Liao, *et al.*, Artificially Engineered Cubic Iron Oxide Nanoparticle as a High-Performance Magnetic Particle Imaging Tracer for Stem Cell Tracking, *ACS Nano*, 2020, **14**(2), 2053–2062, DOI: 10.1021/acsnano.9b08660.

9 F. Chen, E. R. Zhao, G. Hableel, *et al.*, Increasing the Efficacy of Stem Cell Therapy via Triple-Function Inorganic Nanoparticles, *ACS Nano*, 2019, **13**(6), 6605–6617, DOI: 10.1021/acsnano.9b00653.

10 S. Vosen, S. Rieck, A. Heidsieck, *et al.*, Vascular repair by circumferential cell therapy using magnetic nanoparticles and tailored magnets, *ACS Nano*, 2016, **10**(1), 369–376, DOI: 10.1021/acsnano.5b04996.

11 M. Dessale, G. Mengistu and H. M. Mengist, Nanotechnology: A Promising Approach for Cancer Diagnosis, Therapeutics and Theragnosis, *Int. J. Nanomed.*, 2022, **17**, 3735–3749, DOI: 10.2147/IJN.S378074.

12 J. Ge, K. Liu, W. Niu, *et al.*, Gold and gold-silver alloy nanoparticles enhance the myogenic differentiation of myoblasts through p38 MAPK signaling pathway and promote in vivo skeletal muscle regeneration, *Biomaterials*, 2018, **175**, 19–29, DOI: 10.1016/j.biomaterials.2018.05.027.

13 R. Zhang, P. Lee, V. C. H. Lui, *et al.*, Silver nanoparticles promote osteogenesis of mesenchymal stem cells and improve bone fracture healing in osteogenesis mechanism mouse model, *Nanomedicine*, 2015, **11**(8), 1949–1959, DOI: 10.1016/j.nano.2015.07.016.

14 J. Bramhill, S. Ross and G. Ross, Bioactive nanocomposites for tissue repair and regeneration: A review, *Int. J. Environ. Res. Public Health*, 2017, **14**(1), 66, DOI: 10.3390/ijerph14010066.

15 M. A. Yamoah, M. Moshref, J. Sharma, *et al.*, Highly efficient transfection of human induced pluripotent stem cells using magnetic nanoparticles, *Int. J. Nanomed.*, 2018, **13**, 6073–6078, DOI: 10.2147/IJN.S172254.

16 M. A. Yamoah, P. N. Thai and X. D. Zhang, Transgene Delivery to Human Induced Pluripotent Stem Cells Using Nanoparticles, *Pharmaceuticals*, 2021, **14**(4), 334, DOI: 10.3390/ph14040334.

17 H. I. Seo, A. N. Cho, J. Jang, D. W. Kim, S. W. Cho and B. G. Chung, Thermo-responsive polymeric nanoparticles for enhancing neuronal differentiation of human induced pluripotent stem cells, *Nanomedicine*, 2015, **11**(7), 1861–1869, DOI: 10.1016/j.nano.2015.05.008.

18 A. Ito, K. Yoshioka, S. Masumoto, *et al.*, Magnetic heating of nanoparticles as a scalable cryopreservation technology for human induced pluripotent stem cells, *Sci. Rep.*, 2020, **10**(1), 13605, DOI: 10.1038/s41598-020-70707-6.

19 R. Ravichandran, R. Sridhar, J. R. Venugopal, S. Sundarrajan, S. Mukherjee and S. Ramakrishna, Gold nanoparticle loaded hybrid nanofibers for cardiogenic differentiation of stem cells for infarcted myocardium regeneration, *Macromol. Biosci.*, 2014, **14**(4), 515–525, DOI: 10.1002/mabi.201300407.

20 W. K. Ko, D. N. Heo, H. J. Moon, *et al.*, The effect of gold nanoparticle size on osteogenic differentiation of adipose-derived stem cells, *J. Colloid Interface Sci.*, 2015, **438**, 68–76, DOI: 10.1016/j.jcis.2014.08.058.

21 H. Qin, C. Zhu, Z. An, *et al.*, Silver nanoparticles promote osteogenic differentiation of human urine-derived stem cells at noncytotoxic concentrations, *Int. J. Nanomed.*, 2014, **9**(1), 2469–2478, DOI: 10.2147/IJN.S59753.

22 M. Sekuła-Stryjewska, S. Noga, M. Dźwigońska, *et al.*, Graphene-based materials enhance cardiomyogenic and angiogenic differentiation capacity of human mesenchymal stem cells in vitro – Focus on cardiac tissue regeneration, *Mater. Sci. Eng. C*, 2021, **119**, 111614, DOI: 10.1016/j.msec.2020.111614.

23 S. Poussard, M. Decossas, O. Le Bihan, S. Mornet, G. Naudin and O. Lambert, Internalization and fate of silica nanoparticles in C2C12 skeletal muscle cells: Evidence of a beneficial effect on myoblast fusion, *Int. J. Nanomed.*, 2015, **10**, 1479–1492, DOI: 10.2147/IJN.S74158.

24 S. Shamaila, A. K. L. Sajjad, A. Ryma N ul, *et al.*, Advancements in nanoparticle fabrication by hazard free eco-friendly green routes, *Appl. Mater. Today*, 2016, **5**, 150–199, DOI: 10.1016/j.apmt.2016.09.009.

25 A. V. Rane, K. Kanny, V. K. Abitha, S. Thomas and S. Thomas, Methods for Synthesis of Nanoparticles and Fabrication of Nanocomposites, in *Synthesis of Inorganic Nanomaterials: Advances and Key Technologies*, Elsevier, 2018, pp. 121–139, DOI: 10.1016/B978-0-08-101975-7.00005-1.

26 T. Baati, A. Al-Kattan, M. A. Esteve, *et al.*, Ultrapure laser-synthesized Si-based nanomaterials for biomedical applications: In vivo assessment of safety and biodistribution, *Sci. Rep.*, 2016, **6**, 2045–2322, DOI: 10.1038/srep25400.

27 D. Zhang, B. Gökce and S. Barcikowski, Laser Synthesis and Processing of Colloids: Fundamentals and Applications, *Chem. Rev.*, 2017, **117**(5), 3990–4103, DOI: 10.1021/acs.chemrev.6b00468.

28 A. Al-Kattan, D. Grojo, C. Drouet, *et al.*, Short-Pulse Lasers: A Versatile Tool in Creating Novel Nano-/Micro-Structures and Compositional Analysis for Healthcare and Wellbeing Challenges, *Nanomaterials*, 2021, **11**(3), 712, DOI: 10.3390/nano11030712.

29 M. Arora and E. Arora, The Promise of Silicon: bone regeneration and increased bone density, *J. Arthrosc. Jt. Surg.*, 2017, **4**(3), 103–105, DOI: 10.1016/j.jajs.2017.10.003.

30 C. RoyChaudhuri, A review on porous silicon based electrochemical biosensors: Beyond surface area enhancement factor, *Sens. Actuators, B*, 2015, **210**, 310–323, DOI: 10.1016/j.snb.2014.12.089.

31 A. Al-Kattan, Y. V. Ryabchikov, T. Baati, *et al.*, Ultrapure laser-synthesized Si nanoparticles with variable oxidation states for biomedical applications, *J. Mater. Chem. B*, 2016, **4**(48), 7852–7858, DOI: 10.1039/c6tb02623k.

32 A. Al-Kattan, G. Tselikov, K. Metwally, A. A. Popov, S. Mensah and A. V. Kabashin, Laser Ablation-Assisted Synthesis of Plasmonic Si@Au Core-Satellite Nanocomposites for Biomedical Applications, *Nanomaterials*, 2021, **11**(3), 592, DOI: 10.3390/nano11030592.

33 K. P. Tamarov, L. A. Osminkina, S. V. Zinovyev, *et al.*, Radio frequency radiation-induced hyperthermia using Si nanoparticle-based sensitizers for mild cancer therapy, *Sci. Rep.*, 2014, **4**(1), 7034, DOI: 10.1038/srep07034.

34 A. Al-Kattan, M. A. L. Ali, M. Daurat, E. Mattana and M. Gary-Bobo, Biological Assessment of Laser-Synthesized Silicon Nanoparticles Effect in Two-Photon Photodynamic Therapy on Breast Cancer MCF-7 Cells, *Nanomaterials*, 2020, **10**(8), 1462, DOI: 10.3390/nano10081462.

35 A. Al-Kattan, V. Nirwan, A. Popov, *et al.*, Recent Advances in Laser-Ablative Synthesis of Bare Au and Si Nanoparticles and Assessment of Their Prospects for Tissue Engineering Applications, *Int. J. Mol. Sci.*, 2018, **19**(6), 1563, DOI: 10.3390/ijms19061563.

36 S. Testa, P. D'Addabbo, E. Fornetti, *et al.*, Myoblast myogenic differentiation but not fusion process is inhibited via MyoD tetraplex interaction, *Oxid. Med. Cell. Longevity*, 2018, **2018**, 7640272, DOI: 10.1155/2018/7640272.

37 A. Reggio, M. Rosina, N. Krahmer, *et al.*, Metabolic reprogramming of fibro/adipogenic progenitors facilitates muscle regeneration, *Life Sci. Alliance*, 2020, **3**(3), e202000646, DOI: 10.26508/lsa.202000660.

38 E. Fornetti, S. Testa, F. De Paolis, *et al.*, Dystrophic Muscle Affects Motoneuron Axon Outgrowth and NMJ Assembly, *Adv. Mater. Technol.*, 2022, **7**(7), 2101216, DOI: 10.1002/admt.202101216.

39 S. Testa, C. S. Riera, E. Fornetti, *et al.*, Skeletal Muscle-Derived Human Mesenchymal Stem Cells: Influence of Different Culture Conditions on Proliferative and Myogenic Capabilities, *Front. Physiol.*, 2020, **11**, 553198, DOI: 10.3389/fphys.2020.553198.

40 C. Gargioli, G. Turturici, M. M. Barreca, *et al.*, Oxidative stress preconditioning of mouse perivascular myogenic progenitors selects a subpopulation of cells with a distinct survival advantage in vitro and in vivo article, *Cell Death Dis.*, 2018, **9**(1), 1, DOI: 10.1038/s41419-017-0012-9.

41 K. J. Livak and T. D. Schmittgen, Analysis of relative gene expression data using real-time quantitative PCR and the 2-ΔΔCT method, *Methods*, 2001, **25**(4), 402–408, DOI: 10.1006/meth.2001.1262.

42 V. Ramalingam and I. Hwang, Zinc oxide nanoparticles promoting the formation of myogenic differentiation into myotubes in mouse myoblast C2C12 cells, *J. Ind. Eng. Chem.*, 2020, **83**, 315–322, DOI: 10.1016/j.jiec.2019.12.004.

43 D. Böcking, O. Wiltschka, J. Niinimäki, *et al.*, Mesoporous silica nanoparticle-based substrates for cell directed delivery of Notch signalling modulators to control myoblast differentiation, *Nanoscale*, 2014, **6**(3), 1490–1498, DOI: 10.1039/C3NR04022D.

44 Y. W. Huang, M. Cambre and H. J. Lee, The Toxicity of Nanoparticles Depends on Multiple Molecular and Physicochemical Mechanisms, *Int. J. Mol. Sci.*, 2017, **18**(12), 2702, DOI: 10.3390/ijms18122702.

45 M. Kersting, M. Olejnik, N. Rosenkranz, *et al.*, Subtoxic cell responses to silica particles with different size and shape, *Sci. Rep.*, 2020, **10**(1), 21591, DOI: 10.1038/s41598-020-78550-5.

46 S. Behzadi, V. Serpooshan, W. Tao, *et al.*, Cellular uptake of nanoparticles: Journey inside the cell, *Chem. Soc. Rev.*, 2017, **46**(14), 4218–4244, DOI: 10.1039/c6cs00636a.

47 S. W. Ha, M. Neale Weitzmann and G. R. Beck, Bioactive silica nanoparticles promote osteoblast differentiation through stimulation of autophagy and direct association with LC3 and p62, *ACS Nano*, 2014, **8**(6), 5898–5910, DOI: 10.1021/nn5009879.

48 M. Cargnello and P. P. Roux, Activation and Function of the MAPKs and Their Substrates, the MAPK-Activated Protein Kinases, *Microbiol. Mol. Biol. Rev.*, 2011, **75**(1), 50–83, DOI: 10.1128/mmbr.00031-10.

49 A. Keren, Y. Tamir and E. Bengal, The p38 MAPK signaling pathway: A major regulator of skeletal muscle development, *Mol. Cell. Endocrinol.*, 2006, **252**(1–2), 224–230, DOI: 10.1016/j.mce.2006.03.017.